

## Facile synthesis of graphitic carbons decorated with SnO<sub>2</sub> nanoparticles and their application as high capacity lithium-ion battery anodes

A. Ponrouch,<sup>a</sup> M. Sevilla,<sup>b</sup> E. Marchante,<sup>a</sup> M.R. Palacín,<sup>a,\*</sup> A.B. Fuertes<sup>b,\*</sup>

<sup>a</sup> Institut de Ciència de Materials de Barcelona, (ICMAB-CSIC), Campus de la UAB 08193 Bellaterra, Catalonia (Spain)

<sup>b</sup> Instituto Nacional del Carbón (CSIC), P.O. Box 73, 33080 Oviedo, Spain

\* Corresponding author: Tel.: + 34 935801853, fax: + 34 935805729, E-mail address: [rosa.palacin@icmab.es](mailto:rosa.palacin@icmab.es) (M.R. Palacín); Tel.: +34 985118970, fax: +34 985297662, E-mail address: [abefu@incar.csic.es](mailto:abefu@incar.csic.es) (A.B. Fuertes)

### Abstract

A facile and potentially scalable synthesis route to obtain SnO<sub>2</sub>-carbon composites was developed. SnO<sub>2</sub> nanoparticles were deposited on the surface of two types of graphitic carbon: a) commercial porous graphite (HG) and b) graphitic carbon nanostructures (GCN). The synthesis procedure consists of two simple steps: i) room temperature formation/deposition of SnO<sub>2</sub> nanocrystals and ii) thermal treatment at 350 °C in order to generate SnO<sub>2</sub> nanoparticles (size ~ 3.5 nm) over the carbon surface. The electrochemical performance of the graphitic carbons and the SnO<sub>2</sub>-carbon composites as anode materials in Li-ion rechargeable batteries was investigated. In all cases, tape casting electrode fabrication allowed almost full active material utilization. Good cyclabilities were achieved, with HG and HG-SnO<sub>2</sub> showing capacities of 356 and 545 mAh g<sup>-1</sup> respectively after 50 cycles.

**Keywords:** Lithium ion battery; Graphitic carbon; SnO<sub>2</sub>; composite

## 1. Introduction

Although lithium ion batteries are already well established in the market and used in a wide range of applications, the quest for higher energy density has led scientists to search for alternatives to the standard electrode materials [1]. For the negative electrode, materials that react via conversion reactions ( $M_aX_b$ , M being a transition metal and X = O, S, P, N, ...) [2] and materials that electrochemically form alloys with Li (Si, Sn, Sb, Al ...), [3, 4], have been identified as possible alternatives to carbonaceous negative electrodes. However, alloy-based materials generally suffer from low capacity retention due to the substantial changes in volume that accompany the alloying/de-alloying process. This problem has been addressed by adopting a number of strategies [5], including: i) downsizing the particles to the nanoscale [6], ii) use of binary compounds containing elements that do not react with Li and act as non reactive matrix [7], iii) use of carbon coating to improve electrical conductivity and to induce a strain force on the active material [8, 9] and iv) formulation of the electrode modifying the nature of the binder, the carbon additives, etc [10, 11, 12, 13, 14]. Among these strategies, the use of nanocomposites containing tin-based compounds (i. e. Sn, SnO<sub>2</sub> and Sn alloys) embedded in a carbonaceous matrix that acts as buffer against any expansion in volume has been the most effective. Indeed, even though the capacity values observed for such electrodes are well below those that might be expected for pure tin, they are significantly higher than those exhibited by standard carbonaceous electrodes. Thus, several studies have been undertaken to develop fabrication procedures for composites containing carbon and tin compounds, fundamentally Sn and SnO<sub>2</sub>. To date, most of the reports have focussed on the influence on electrode performance exerted by: i) the type of carbon used as support (e. g. carbon microbeads, nanotubes, graphene, graphite,

etc) [15, 16, 17, 18], ii) the procedure employed to synthesize the tin oxide nanoparticles (hydrothermal, microwave, etc) [18, 19], iii) the amount of tin oxide deposited onto the carbon surface [20] and iv) the effect of alloying tin with other active or inactive elements [21, 22].

The procedures used to synthesize SnO<sub>2</sub>-carbon composites for their application in lithium ion batteries are generally complex [19, 23, 24, 25]. Moreover, most effective composites use sophisticated non-commercial materials as carbon supports, such as carbon capsules [26], templated mesoporous carbons [27], carbon nanotubes [28] or graphene [29]. These circumstances severely limit the scalability and mass production of SnO<sub>2</sub>-carbon composites. Hence, the development of simple and potentially scalable synthesis strategies to fabricate SnO<sub>2</sub>-carbon composites represents an important challenge. In this paper, an easy and potentially scalable procedure for synthesizing SnO<sub>2</sub>-carbon composites by means of an inexpensive and rapid method for incorporating uniform SnO<sub>2</sub> nanoparticles (size < 4 nm) onto the surface of highly crystallized carbons is reported. Two types of carbon support were used: a) a commercially available porous graphite and b) highly graphitized nanocarbons fabricated by means of a simple procedure as reported elsewhere [30]. The SnO<sub>2</sub>-carbon composites thus obtained were tested in lithium batteries. The effect of the electrode formulation procedure was also ascertained by comparing powder electrode technology (a simple mixture consisting of a carbon additive and a tin-based powder material) with tape casted composite electrodes (fabricated with the aid of a binder).

## 2. Experimental

### 2.1. Materials preparation

Two types of graphitic carbons were used in these experiments: i) a commercial porous graphite TIMREX HSAG-300 (Timcal), here denoted as HG, and ii) graphitic carbon nanostructures prepared in our laboratory and denoted as GCN. The preparation of the GCN material has been reported in detail elsewhere [30]. Briefly, it consists of the following steps: a) the pyrolysis of Fe(II) gluconate dihydrate (Aldrich) under nitrogen up to 900°C for 3 hours, b) treating the carbon-iron composite under reflux for 2 hours in an acid solution of potassium permanganate with a composition (mol ratios) of H<sub>2</sub>O : H<sub>2</sub>SO<sub>4</sub> : KMnO<sub>4</sub> = 1 : 0.02 : 0.006, c) separation of the solid product by centrifugation and its treatment with HCl (10%) to remove the MnO<sub>2</sub> formed. After being collected by centrifugation, the solid was washed with abundant distilled water and ethanol. This product is composed almost exclusively of graphitic carbon nanostructures (GCN).

The incorporation of SnO<sub>2</sub> nanoparticles into the graphitic carbon samples was carried out using the procedure reported by Cao et al. [31]. In a typical synthesis, 100 mg of graphitic carbon was dispersed in a solution containing 175 mL of water, 3 mL of HCl (37%) and 3.5 g SnCl<sub>2</sub> (Aldrich). The dispersion was sonicated for 45 min and then stirred for 3.5 h at room temperature. The solid sample was collected by centrifugation, washed with abundant distilled water and dried at 120 °C. Finally, the SnO<sub>2</sub>-carbon composites were thermally treated under nitrogen up to 350 °C (5 °C min<sup>-1</sup>) for 4 h. The final products were denoted as HG-SnO<sub>2</sub> or GCN-SnO<sub>2</sub> depending on the type of graphitic carbon used.

## 2.2. Characterization of materials

X-ray diffraction (XRD) patterns of the graphitic carbons and graphite-SnO<sub>2</sub> decorated composite were obtained on a Siemens D5000 instrument operating at 40 kV and 20 mA, using CuK $\alpha$  radiation. Adsorption measurements of the samples were performed using a Micromeritics ASAP 2020 volumetric adsorption system. The external surface area ( $S_{\text{ext}}$ ) was estimated by means of the  $\alpha_s$ -plot method and a non-graphitized carbon black was used as reference [32]. The loadings of SnO<sub>2</sub> into the graphite-SnO<sub>2</sub> decorated composite were determined by thermogravimetric analysis (TGA), which was performed in a C. I. Electronics system under air (heating rate: 10 °C min<sup>-1</sup>). The morphology of the carbons and composites was examined by scanning (SEM, Zeiss DSM 942) and transmission (TEM, JEOL-2000 FXII) electron microscopy.

## 2.3. Electrochemical measurements

Two different procedures were used for the fabrication of the composite electrode: i) 85% of the active material (referred to hereafter as AM), i. e. GCN, HG, GCN-SnO<sub>2</sub> or HG-SnO<sub>2</sub>, was gently mixed with 15% of Super P carbon (referred to hereafter as Csp from Timcal) by magnetic stirring in cyclohexane overnight, followed by solvent evaporation (denoted powdered electrodes), and ii) a slurry prepared by mixing 80 wt.% of AM, 10 wt.% of PVDF as a binder and 10 wt.% of Csp in *N*-Methylpyrrolidone (NMP, Aldrich) was tape casted on a 20  $\mu\text{m}$  thick copper foil (Goodfellow) with a 250  $\mu\text{m}$  Doctor-Blade and then subjected to further drying at 120 °C under vacuum (denoted tape casted electrodes).

Swagelok-type cells were then assembled with the working electrode being composed either of i) 5 mg of the composite powder or ii) 0.8 cm<sup>2</sup> disk electrodes cut from the tape

(typical loading ranging between 1 and 2 mg cm<sup>-2</sup>) and pressed at 6 tons. A disk of Li metal foil (Chemetal) was used as counter and reference electrode. Two sheets of Whatman GF/d borosilicate fiber glass were used as separator, which was soaked with the electrolyte (ca. 0.5 cm<sup>3</sup> of 1 M LiPF<sub>6</sub> in EC:DMC 1:1 (LP30, Merck)). Electrochemical cycling experiments were carried out in galvanostatic mode with potential limitation (GCPL) between 0.01 and 2 V vs. Li<sup>+</sup>/Li, at a rate of C/10 (i.e. 1 Li<sup>+</sup> in 10 h), using either an Arbin BT2042 or a MacPile II potentiostat. All the capacities presented here were determined upon reduction and were calculated with respect to the total electrode mass, i.e. per gram of C for HG and GCN and per gram of carbon + SnO<sub>2</sub> for HG-SnO<sub>2</sub> and GCN-SnO<sub>2</sub>.

### **3. Results and Discussion**

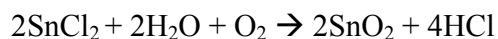
#### **3.1. Physical properties of the graphitic carbons and graphite-SnO<sub>2</sub> decorated composites**

The microstructure of the graphitic carbons and the graphite-SnO<sub>2</sub> decorated composites was investigated by SEM, TEM, X-ray diffraction analysis and gas adsorption measurements. The GCN synthesis method has been described in a previous work [30]. The SEM image in Figure 1a shows that the GCN sample is composed of rod-like nanoparticles (length up to 1 μm, diameter: ~ 100 – 150 nm). TEM examination of these nano-rods reveals a corrugated tubular-like morphology and a shell thickness of around 10 - 25 nm (see inset in Fig. 1a and Fig. 1b). These walls have a high crystallinity, as illustrated by the high-resolution transmission electronic microscopy image in Figure 1b, which displays well defined (002) lattice fringes. The X-ray diffraction pattern of GCN confirms that this material is highly graphitic (Figure 2a), exhibiting well-resolved XRD peaks characteristic of a graphitic structure. The structural parameters of the GCN (i.e. d-spacing (002) and the

crystallite sizes along the c-axis,  $L_c$ , and a-axis,  $L_a$ , were estimated. The value obtained for the d-spacing (0.339 nm) is larger than the graphite value (0.3354 nm), suggesting that the stacking of the graphene layers has experienced some distortion (turbostratic structure). The sizes of the graphitic crystallites  $L_c$  and  $L_a$  are around 10 nm and 27 nm, respectively. The HG graphite also exhibits high crystallinity, as evidenced by the XRD pattern in Figure 2a, where  $d(002) = 0.336$  nm and the values of the crystallite sizes  $L_c$  and  $L_a$  are 16 nm and 41 nm respectively.

The  $N_2$  sorption isotherm corresponding to GCN exhibits a large nitrogen adsorption uptake at relative pressures  $> 0.99$  (see Figure 3a), which is typical of nanosized materials that do not contain any framework-confined pores. This result is consistent with the morphology of the GCN, as illustrated by SEM and TEM images (Fig. 1a). In the case of the GCN sample, the adsorption only occurs at the outer surface of the nanoparticles so that not surprisingly the BET surface area ( $96 \text{ m}^2 \text{ g}^{-1}$ ) matches the external surface area, as deduced from the  $\alpha_s$ -plot analysis ( $102 \text{ m}^2 \text{ g}^{-1}$ ). Given that this material does not contain any internal porosity, it can be inferred that the  $\text{SnO}_2$  nanoparticles are deposited exclusively on the outer surface, a characteristic which favors their accessibility to electrolytes and, in consequence, their application in electrochemical devices such as Li-ion batteries. In the case of the HG graphite, however only  $\sim 40\%$  of the BET surface area ( $310 \text{ m}^2 \text{ g}^{-1}$ ) can be ascribed to the external surface, the rest being associated to the framework-confined pores ( $> 2$  nm), as can be seen from the  $\alpha_s$ -plot analysis applied to the  $N_2$  sorption isotherm (Figure 3b).

During the liquid-phase synthesis step, the formation of tin oxide takes place via the oxidation of  $\text{Sn}^{2+}$  at the surface of the carbon particles and its precipitation as  $\text{SnO}_2$  nanocrystals. The overall reaction can be written as:



Thermogravimetric analysis of the synthesized composites reveals that the amount of  $\text{SnO}_2$  in the composite is 23 wt.% for GCN- $\text{SnO}_2$  and 32 wt.% for HG- $\text{SnO}_2$ . The subsequent thermal treatment of such as-synthesized composites promotes the growth of the primary  $\text{SnO}_2$  nanoclusters into  $\text{SnO}_2$  nanoparticles. These nanoparticles are clearly identified by the XRD patterns (Figure 2b) and TEM images (Figures 1c and 1d). Figure 2b shows the XRD patterns obtained for the GCN- $\text{SnO}_2$  and HG- $\text{SnO}_2$  samples. Both composites exhibit broad peaks, which denote poor crystallinity. These peaks can be assigned to the tetragonal rutile  $\text{SnO}_2$  polymorph (JCPDS card no. 41-1445). The crystallite size was estimated through the Scherrer equation considering the FWHM for the (101) peak. The  $\text{SnO}_2$  crystallite size thus calculated proved to be similar for both composites,  $\sim 3.5$  nm. This value is consistent with the diameter of  $\text{SnO}_2$  particles inferred by TEM inspection (Figures 1c and 1d). Furthermore, these TEM images prove that the  $\text{SnO}_2$  nanoparticles are uniformly distributed over the surface of the carbon supports. The nitrogen sorption isotherms obtained for the GCN- $\text{SnO}_2$  and HG- $\text{SnO}_2$  samples are presented in Figures 3a and 3b respectively. A reduction in  $\text{N}_2$  uptake was observed for both composites in relation to the carbon supports. The BET surface area of the HG-  $\text{SnO}_2$  composite was found to be  $170 \text{ m}^2 \text{ g}^{-1}$ . This BET surface area on a carbon basis is  $\sim 250 \text{ m}^2 \text{ g}^{-1}$ , which indicates a reduction of around 20% of the surface area of the HG sample and suggests that some of the pores in the HG sample are obstructed by the deposited  $\text{SnO}_2$  nanoparticles. In contrast, the BET



surface area of the GCN-SnO<sub>2</sub> sample is 106 m<sup>2</sup> g<sup>-1</sup> (external surface area: 110 m<sup>2</sup> g<sup>-1</sup>), while the surface area on a carbon basis is around 140 m<sup>2</sup> g<sup>-1</sup>. This value is notably higher than the BET surface area of GCN (96 m<sup>2</sup> g<sup>-1</sup>) and indicates that the deposited SnO<sub>2</sub> nanoparticles have a positive contribution to the surface area of the composite in relation to GCN.

### **3.2. Electrochemical performance in lithium cells**

#### 3.2.1. Graphitic carbons

As mentioned in the previous section, the SnO<sub>2</sub>-carbon composites (GCN-SnO<sub>2</sub> and HG-SnO<sub>2</sub>) exhibit SnO<sub>2</sub> contents of 23 wt.% and 32 wt.% respectively and similar particle sizes (ca. 3.5 nm). The main difference between them is the porosity of the graphitic carbon. Indeed, no internal porosity was observed in the case of GCN, while HG is porous to some extent. The voltage-capacity profiles for powdered electrodes prepared from pure GCN and HG graphitic materials are shown in Figure 4A. Both exhibit an irreversible sloppy plateau at ca. 0.8 V vs. Li<sup>+</sup>/Li, corresponding to the formation of a stable SEI during the first cycle [33].

In the case of the pure graphitic carbon electrodes, decomposition of the electrolyte is the main cause of the coulombic inefficiency during the first cycle and is thus proportional to the electrochemically active surface area. The fact that HG and GCN present similar coulombic efficiencies (ca. 25%) irrespective of whether powder or tape technology is used is surprising in view of their very different surface areas (ca. 310 and 96 m<sup>2</sup> g<sup>-1</sup> for HG and GCN, respectively). However, both can be expected to exhibit the same external surface area, as ~ 60% of the surface area of the HG particles is associated with the internal pores. Figure 5 displays a schematic representation of a graphite particle with a uniform pore size.

We estimated an approximate SEI volume considering 1  $\mu\text{m}$  carbon particles with 60% internal porosity and a pore size of 2 nm. Assuming a thickness of 5 nm, the SEI layer [33] volume related to the external surface area is of the order of  $1.6 \times 10^{-14} \text{ cm}^3$  and that ascribed to the internal pores one order of magnitude smaller ( $\sim 2.3 \times 10^{-15} \text{ cm}^3$ ). Hence the irreversible capacity in relation to the formation of the SEI layer within the pores is negligible.

The results shown in Figure 4B (cf. triangle and square symbols) indicate that much higher capacities and lower fading were recorded in the case of the tape casted electrodes thereby confirming that the formulation of the electrode is of prime importance for achieving the best possible electrochemical performance, even when using materials which do not experience significant volume changes such as graphite [34, 35].

### 3.2.2. SnO<sub>2</sub>-carbon composites

As expected, the incorporation of SnO<sub>2</sub> into the graphitic carbon supports produces a substantial increase in the capacities in all cases (see Figure 6). This finding further confirms good electrical contact between the SnO<sub>2</sub> nanoparticles and the graphitic material in the as prepared composites. The results shown in Figure 6B reveal that the potential corresponding to the first discharge sloppy plateau recorded for the SnO<sub>2</sub>-carbon composites is higher than that of the graphitic supports. This is presumably due to irreversible reduction in the case of SnO<sub>2</sub> (ca. 1.1 V vs. Li<sup>+</sup>/Li), which results in the formation of tin metallic nanoparticles prior to the formation of Li-Sn alloys [36].

Larger capacity values were obtained with HG-SnO<sub>2</sub> and GCN-SnO<sub>2</sub> powder electrodes, which exhibit first discharge capacities higher than 1200 mAh g<sup>-1</sup> (cf. 600 and 400 mAh g<sup>-1</sup> for HG and GCN respectively). A similar trend was observed for the tape technology: HG

and GCN exhibited first discharge capacities of about 1530 and 1100 mAh g<sup>-1</sup> while capacities larger than 1800 mAh g<sup>-1</sup> were recorded in the case of the SnO<sub>2</sub>-C composites. Coulombic efficiencies were also observed to increase: 25% in the case of the graphitic carbons and > 30% for the SnO<sub>2</sub>-carbon composites (see insets in Figures 4A and 6A). Slightly higher values were recorded in the case of HG-SnO<sub>2</sub> compared to the GCN-SnO<sub>2</sub> powder electrodes (ca. 43% versus 33%, respectively), most probably due to the slightly higher SnO<sub>2</sub> content in HG-SnO<sub>2</sub> compared to GCN-SnO<sub>2</sub>. Figure 6B shows the evolution of capacity upon cycling for HG-SnO<sub>2</sub> and GCN-SnO<sub>2</sub>. Larger capacities with lower fading during cycling were observed for both samples in the case of electrode preparation *via* tape technology. Figure 7 displays the plot of capacity versus cycle number for the graphitic carbons and the SnO<sub>2</sub>-carbon composite tape electrodes over long term cycling. Better capacity retention is observed for HG, with values as high as ca. 356 mAh g<sup>-1</sup> after 50 cycles (compared to 295 mAh g<sup>-1</sup> being recorded for GCN, see Figure 7). This suggests that the porous structure of HG allows easier access to the bulk of the material thereby facilitating the intercalation/deintercalation. Similar differences were observed in the case of the HG-SnO<sub>2</sub> and GCN-SnO<sub>2</sub> composites, their capacities being 545 mAh g<sup>-1</sup> and 400 mAh g<sup>-1</sup> respectively after 50 cycles. These values are close to the calculated theoretical capacities for the composite electrodes (570 mAh g<sup>-1</sup> for HG-SnO<sub>2</sub> and 515 mAh g<sup>-1</sup> for GCN-SnO<sub>2</sub>, which are estimated considering the respective compositions and from the respective theoretical capacities of graphite and SnO<sub>2</sub>). As both materials show good capacity retention, the difference between their specific capacities is probably due to the easier access to the bulk of the material in the case of HG and to the slightly higher SnO<sub>2</sub> content in the case of HG-SnO<sub>2</sub> (32 wt.%). Overall, these results demonstrate the benefits of tape electrode technology, which allows the achievement of almost the theoretical full

capacity for both composites, yielding values that are comparable to the best results found in the literature. Indeed, previously reported specific capacities of around 500 mAh g<sup>-1</sup> are scarce even though the synthesis protocols usually involved more complex and costly procedures [16,17,19,23,24,25].

#### **4. Conclusions**

A facile, inexpensive and potentially scalable procedure for the synthesis of SnO<sub>2</sub>-carbon composites made up of tin oxide nanoparticles that are deposited onto the surface of two types of graphitic carbon is presented. The deposited SnO<sub>2</sub> nanoparticles are highly uniform in size (~ 3.5 nm) and they are homogeneously distributed over the surface of the carbon supports. The effectiveness of this synthesis strategy has been demonstrated by applying it to two graphitic carbons with different structural properties, i. e. commercial porous graphite and non-porous graphitic carbon nanocoils prepared in our laboratory. The porosity of the graphite was found to have a significant influence on the irreversible capacity loss on the first cycle, since the formation of the SEI layer is hindered inside the small pores. The tape electrodes containing SnO<sub>2</sub>-carbon composites exhibit very good electrochemical performance against lithium. Indeed capacities of 545 mAh g<sup>-1</sup> for HG-SnO<sub>2</sub> and 400 mAh g<sup>-1</sup> for GCN-SnO<sub>2</sub> were recorded after 50 cycles. These values are significantly larger than those obtained with bare graphitic supports (356 mAh g<sup>-1</sup> for HG and 295 mAh·g<sup>-1</sup> for GCN) and compare very well with the results reported in previous published works for composites obtained using complex, time consuming methods where specific capacities of around 500 mAh g<sup>-1</sup> are scarce.

**Acknowledgments.** We acknowledge the financial support received from the Spanish Ministry of Science and Innovation (MAT2011-24757 and MAT2008-00407). M. S. thanks the Spanish Ministry of Science and Innovation for the award of a Postdoctoral Mobility contract.

## References

---

1. Palacín MR (2009) Recent advances in rechargeable battery materials: a chemist's perspective. *Chem Soc Rev* 38:2565-2575
2. Cabana J, Monconduit L, Larcher D, Palacín MR (2010) Beyond Intercalation-Based Li-Ion Batteries: The State of the Art and Challenges of Electrode Materials Reacting Through Conversion Reactions. *Adv Mater* 22:E170-E192
3. Park CM, Kim JM, Kim H, Sohn HJ (2010) Li-alloy based anode materials for Li secondary batteries. *Chem Soc Rev* 39:3115-3141.
4. Zhang WJ (2011) A review of the electrochemical performance of alloy anodes for lithium-ion batteries. *J Power Sources* 196:13-24
5. Larcher D, Beattie S, Morcrette M, Edström K, Jumas JC, Tarascon JM (2007) Recent findings and prospects in the field of pure metals as negative electrodes for Li-ion batteries. *J Mater Chem* 17:3759-3772.
6. Bruce PG, Scrosati B, Tarascon JM (2008) Nanomaterials for Rechargeable Lithium Batteries. *Angew Chem Int Ed* 47:2930-2946.
7. Beaulieu LY, Dahn JR (2000) The reaction of lithium with Sn-Mn-C intermetallics prepared by mechanical alloying. *J Electrochem Soc* 147:3237-3241
8. Ryu JH, Kim JW, Sung YE, Oh SM (2004) Failure Modes of Silicon Powder Negative Electrode in Lithium Secondary Batteries. *Electrochem Solid-State Lett* 7:A306-A309
9. Saint J, Morcrette M, Larcher D, Laffont L, Beattie S, Pérès JP, Talaga D, Couzi M, Tarascon JM (2007) Towards a fundamental understanding of the improved electrochemical performance of silicon-carbon composites. *Adv Funct Mater* 17:1765-1774

- 
10. Sivasankaran V, Marino C, Chamas M, Soudan P, Guyomard D, Jumas JC, Lippens PE, Monconduit L, Lestriez B (2011) Improvement of intermetallics electrochemical behavior by playing with the composite electrode formulation. *J Mater Chem* 21:5076-5082
  11. Lestriez B (2010) Functions of polymers in composite electrodes of lithium ion batteries. *C R Chimie* 13:1341-1350
  12. Li J, Dahn HM, Krause LJ, Le DB, Dahn JR (2008) Impact of binder choice on the performance of  $\alpha$ -Fe<sub>2</sub>O<sub>3</sub> as a negative electrode. *J Electrochem Soc* 155:A812-A816
  13. Lestriez B, Desaeveer S, Danet J, Moreau P, Plée D, Guyomard D (2009) Hierarchical and Resilient Conductive Network of Bridged Carbon Nanotubes and Nanofibers for High-Energy Si Negative Electrodes. *Electrochem Solid-State Lett* 12:A76-A80
  14. Jiang C, Ichihara M, Honma I, Zhou H (2007) Effect of particle dispersion on high rate performance of nano-sized Li<sub>4</sub>Ti<sub>5</sub>O<sub>12</sub> anode. *Electrochim Acta* 52:6470-6475
  15. Wang Y, Su F, Lee JY, Zhao XS (2006) Crystalline Carbon Hollow Spheres, Crystalline Carbon-SnO<sub>2</sub> Hollow Spheres, and Crystalline SnO<sub>2</sub> Hollow Spheres: Synthesis and Performance in Reversible Li-Ion Storage. *Chem Mater* 18:1347-1353
  16. Fu Y, Ma R, Shu Y, Cao Z, Ma X (2009) Preparation and characterization of SnO<sub>2</sub>/carbon nanotube composite for lithium ion battery applications. *Mater Lett* 63:1946-1948
  17. Du Z, Yin X, Zhang M, Hao Q, Wang Y, Wang T (2010) In situ synthesis of SnO<sub>2</sub>/graphene nanocomposite and their application as anode material for lithium ion battery. *Mater Lett* 64:2076-2079
  18. Courtel FM, Baranova EA, Abu-Lebdeh Y, Davidson IJ (2010) In situ polyol-assisted synthesis of nano-SnO<sub>2</sub>/carbon composite materials as anodes for lithium-ion batteries. *J Power Sources* 195:2355-2361
  19. Lou XW, Chen JS, Chen P, Archer LA (2009) One-Pot Synthesis of Carbon-Coated SnO<sub>2</sub> Nanocolloids with Improved Reversible Lithium Storage Properties. *Chem Mater* 21:2868-2874

- 
20. Li MY, Liu CL, Wang Y, Dong WS (2011) Simple Synthesis of Carbon/Tin Oxide Composite as Anodes for Lithium-Ion Batteries. *J Electrochem Soc* 158:A296-A301
  21. Park CM, Jeon KJ (2011) Porous structured SnSb/C nanocomposites for Li-ion battery anodes. *Chem Commun* 47:2122-2124
  22. Li MY, Liu CL, Shi MR, Dong WS (2011) Nanostructure Sn–Co–C composite lithium ion battery electrode with unique stability and high electrochemical performance. *Electrochim Acta* 56:3023-3028
  23. Chen JS, Cheah YL, Chen YT, Jayaprakash N, Madhavi S, Yang YH, Lou XW (2009) SnO<sub>2</sub> Nanoparticles with Controlled Carbon Nanocoating as High-Capacity Anode Materials for Lithium-Ion Batteries. *J Phys Chem C* 113:20504-20508
  24. Chou SL, Wang JZ, Zhong C, Rahman MM, Liu HK, Dou SX (2009) A facile route to carbon-coated SnO<sub>2</sub> nanoparticles combined with a new binder for enhanced cyclability of Li-ion rechargeable batteries. *Electrochim Acta* 54:7519-7524
  25. Liu H, Long D, Liu X, Qiao W, Zhan L, Ling L (2009) Facile synthesis and superior anodic performance of ultrafine SnO<sub>2</sub>-containing nanocomposites. *Electrochim Acta* 54:5782-5788
  26. Lou XW, Li CM, Archer LA (2009) Designed Synthesis of Coaxial SnO<sub>2</sub>@carbon Hollow Nanospheres for Highly Reversible Lithium Storage. *Adv Mater* 21:2536-2539
  27. Fan J, Wang T, Yu C, Tu B, Yiang Z, Zhao DY (2004) Ordered, Nanostructured Tin-Based Oxides/Carbon Composite as the Negative-Electrode Material for Lithium-Ion Batteries. *Adv Mater* 16:1432-1436
  28. Wang Y, Zeng HC, Lee JY (2006) Highly Reversible Lithium Storage in Porous SnO<sub>2</sub> Nanotubes with Coaxially Grown Carbon Nanotube Overlayers. *Adv Mater* 18:645-649
  29. Paek SM, Yoo EJ, Honma I (2009) Enhanced Cyclic Performance and Lithium Storage Capacity of SnO<sub>2</sub>/Graphene Nanoporous Electrodes with Three-Dimensionally Delaminated Flexible Structure. *Nano Lett* 9:72-75
  30. Sevilla M, Salinas Martinez-de Lecea C, Valdes-Solis T, Morallon E, Fuertes AB (2008) Solid-phase synthesis of graphitic carbon nanostructures from iron and cobalt

---

gluconates and their utilization as electrocatalyst supports. *Phys Chem Chem Phys* 10:1433-1442

31. Cao Y, Cao J, Liu J, Zheng M, Shen K (2007) Sonochemical Fabrication and Photoluminescence Properties of Ordered Mesoporous Carbon–Tin Oxide Nanocomposites. *Chem Lett* 36:254

32. Kruk M, Jaroniec M, Gadkaree KP (1997) Nitrogen Adsorption Studies of Novel Synthetic Active Carbons. *J Colloid Interf Sci* 192:250-256

33. Aurbach D (2000) Review of selected electrode–solution interactions which determine the performance of Li and Li ion batteries. *J Power Sources* 89:206-218

34. Courtel FM, Niketic S, Duguay D, Abu-Lebdeh Y, Davidson IJ (2011) Water-soluble binders for MCMB carbon anodes for lithium-ion batteries. *J Power Sources* 196:2128-2134

35. Ponrouch A, Palacin MR (2011) On the impact of the slurry mixing procedure in the electrochemical performance of composite electrodes for Li-ion batteries: A case study for mesocarbon microbeads (MCMB) graphite and  $\text{Co}_3\text{O}_4$ . *J Power Sources* 196:9682-9688

36. Courtney IA, Dahn JR (1997) Electrochemical and In Situ X-Ray Diffraction Studies of the Reaction of Lithium with Tin Oxide Composites. *J Electrochem Soc* 144:2045-2052



---

**Figure Captions**

**Fig. 1.** (a) SEM, (a, inset) TEM and (b) HRTEM images of graphitic carbon nanostructures. TEM images of (c) GCN-SnO<sub>2</sub> and (d) HG-SnO<sub>2</sub> composites

**Fig. 2.** XRD patterns of: (a) graphitic carbons and (b) carbon-SnO<sub>2</sub> composites

**Fig. 3.** Nitrogen sorption isotherms of: (a) GCN and GCN-SnO<sub>2</sub>; (b) HG and HG-SnO<sub>2</sub> samples. The GCN isotherm has been vertically shifted by 50 cm<sup>3</sup> g<sup>-1</sup> for clarity

**Fig. 4.** A) Voltage versus capacity profiles for GCN and HG (solid red and black dotted curves respectively), with first cycle coulombic efficiency as inset. B) Capacity versus cycle number for GCN based electrodes (red symbols) and HG based electrodes (black symbols). Square symbols denote powder electrodes and triangle symbols tape casted electrodes. The blue dotted line represents the theoretical capacity of graphite (372 mAh g<sup>-1</sup>)

**Fig. 5.** Schematic representation of the SEI formation in the electrochemically active surface area of a porous carbon particle after the first discharge

**Fig. 6.** A) Voltage versus capacity profiles for GCN-SnO<sub>2</sub> and HG-SnO<sub>2</sub> (solid red and black dotted curves respectively), with first cycle coulombic efficiency as inset. B) Capacity versus cycle number for GCN-SnO<sub>2</sub> based electrodes (red symbols) and HG-SnO<sub>2</sub> based electrodes (black symbols). Square symbols denote powder electrodes and triangle symbols tape casted electrodes. The blue dotted line represents the theoretical capacity of the graphite (372 mAh g<sup>-1</sup>)

**Fig. 7.** Capacity versus cycle number for HG (black triangle), GCN (black square scatters), HG-SnO<sub>2</sub> (red triangle) and GCN-SnO<sub>2</sub> (red square). In all cases the composite electrodes were tape casted. The blue dotted line represents the theoretical capacity of graphite (372 mAh g<sup>-1</sup>)